LLNL-PROC-415121

LAWRENCE
LIVERMORE
NATIONAL
LABORATORY

Dense Plasma Focus Z-pinches for High Gradient Particle Acceleration

V. Tang, M. L. Adams, B. Rusnak

July 28, 2009

36th International Conference on Plasma Science
San Diego, CA, United States
May 31, 2009 through June 5, 2009

Dense Plasma Focus Z-pinches for High Gradient Particle Acceleration

V. Tang, M. L. Adams, and B. Rusnak, Lawrence Livermore National Laboratory, Livermore, CA 94550

Keywords: Accelerators, Particle beams, Plasma focus, Plasma sheaths, Plasma pinch, Plasma applications, Neutron sources

Abstract
The final Z-pinch stage of a Dense Plasma Focus (DPF) could be used as a simple, compact, and potentially rugged plasma-based high-gradient accelerator with fields at the 100 MV/m level. In this paper we review previously published experimental beam data that indicate the feasibility of such an DPF-based accelerator, qualitatively discuss the physical acceleration processes in terms of the induced voltages, and as a starting point examine the DPF acceleration potential by numerically applying a self-consistent DPF system model that includes the induced voltage from both macroscopic and instability driven plasma dynamics. Applications to the remote detection of high explosives and a multi-staged acceleration concept are briefly discussed.

I. Introduction
There is a significant need for compact high gradient ~100 MV/m particle accelerators for a broad range of applications from remote detection of nuclear [1] and explosives materials [2] for National Security to radiotherapy in Health Care [3]. In regards to remote explosives detection, the near-term accelerator requirements are typically in the MeV range for particle energy with average currents in the 10-100 μA range. The ideal accelerator would also be sufficiently compact for field operations and thus require high engineering gradients. For example, a directional D-D neutron source operating at 4 MV with approximately 100 μA of D^+ average current could provide a total neutron output greater than 10^{10} n/s with a forward-to-side (0 and 180 deg.) neutron flux ratio up to 10 for a 20 degree wide cone when a thin target is used. Peak neutron energies of ~7.2 MeV would be emitted in the forward direction. Such a neutron source, if compact enough, could be used for remote explosives detection in the field via Pulsed Fast Neutron Analysis. Neutronics analysis indicates that this directional source could enable remote identification of ~100 lb level explosives at ~10 m distance on the seconds timescale. Accelerator requirements for other detection concept-of-operations (CONOPS) range from 2 MeV protons for very directional neutrons from P-Li reactions for nuclear material identification to, longer-term, GeV level particle beams for much greater stand-off detection. Overall, the availability of a high-gradient, simple, and rugged accelerator would enable numerous CONOPS.

Based on experimental data, the Dense Plasma Focus (DPF) [4-8] has the potential to serve as the basis for such an accelerator for some of the above applications. The DPF is a physically simple device with experimental geometries typically consisting of an open-ended coaxial gun (approximately 1-10 cm long and 1-10 cm diameter) loaded with a static gas and driven by capacitors from 100 J to ~MJ. During operation a plasma sheath is formed from flashover of the coaxial insulator, the sheath is accelerated along the central anode, and when it reaches the end of the anode the sheath collapses or pinches to form a fast Z-pinch [9] on axis. Figure 1 schematically illustrates DPF operation. The length of the central anode is dependent on the speed of the pulsed power driver and serves to couple the power effectively to the DPF Z-pinch; a classical gas-puffed Z-pinch [e.g. 10] is achieved in the limit of zero rundown and contains similar physics. Up to 10^{12} D-D neutrons have been emitted during the pinch phase when DPF machines were operated with deuterium gas. In the pinch, approximately 100 MV/m and greater axial electric fields are formed through nonlinear processes. These fields result in deci-Ampere or greater MeV level ion beams emitted primarily away from the center electrode and kilo-Ampere level electron beams emitted primarily towards the center electrode [11-27]. The MeV level ion beams are emitted in the 10's ns time-scale and can have total charge of approximately 100 μC for larger devices such as the former ~100 kJ, LLNL DPF [12-13] operated with voltages up to 27 kV. Average accelerating gradients in excess of 100 MV/m are observed; for example, ~5 MeV deuterons were emitted from ~2 cm long plasmas in [13]. Local gradients possibly greater than 10 GV/m are observed in some experiments [15]. The beams extracted and accelerated from the plasma typically have energy distributions described by a power law of the form E^{-x} (with x~5 in [20] for example) or a decaying exponential [13]. In fact anisotropic D-D neutron output from DPF are commonly measured and are deduced to be from beam-target reactions caused by the ion beams from these gradients; additionally, calculations based on plasma measurements often indicate thermonuclear reactions to be insufficient [28-36]. Experimental evidence also shows, for some machines, different operating regimes for optimized beam production in terms of current and energy versus maximum neutron production [13]; typically lower operating pressure resulting in faster sheaths favor higher beam energies.

It might be possible to exploit these experimentally observed 100 MV/m level gradients further for a low-cost high-gradient plasma driven accelerator once the gradients are understood. At the MV level, DPFs optimized for beam production and acceleration could, for example, be useful for engineering DPF sources with higher neutron directionality and lower driver energy. Note that the DPF in [13], if it can be operated at ~Hz level, satisfies some of the source requirements discussed above for explosives detection as more than ~10 μC of deuterium ions are emitted with energies in the 2 to 5 MeV range. If DPFs can scale to higher and mono-energetic beam output through staged acceleration of independently injected beams using, for example, multiple stacked DPFs analogous to proposals for staged laser-plasma accelerators [37], the technology might provide a cost-effective and compact accelerator path beyond the 10 to 100's MeV energy level. Mono-energetic particle beams have been injected into DPF plasmas through the device anode in at least one experiment; in Friewald's work [38] a beam was used successfully for plasma heating and increased neutron yield but the work was not oriented towards accelerating the injected beam. In a multi-DPF setup device timing and jitter would clearly be important issues, and DPFs with short anodes would be preferred to maximize effective acceleration gradients.

Previous works on analyzing beam production in DPF and related fast Z-pinches identified various mechanisms that are thought to be responsible for the observed beams [29, 39-48]. These works propose that the high electric fields and accelerating voltage in the pinch stem from a combination of the following: 1) inductively through macroscopic fluid motion from pinch formation; 2) inductively through various plasma instabilities during pinch phase; 3) resistively through a large decrease in plasma conductivity due to microscopic instabilities; and 4) shock physics involved in the colliding plasma sheaths. These studies typically employed local models of the pinch dynamics and a test-particle approach for the accelerated ions and electrons. From a systems point of view, various numerical works have studied the DPF starting from the rundown to the pinch phase usually using a fluid approach [49-52]. In particular there is ongoing work on computationally fast tunable reduced physics systems models [53-57] that have found some success for interpreting experimental results in terms of matching experimental quantities such as measured current. Although these simple system models might not capture all the significant details, especially kinetic based effects, of DPFs, they can be useful as a starting point for understanding experimental results, examining system energy balance and the limits of a fluid approach, and initial parameter scans for more detailed analyses.

As a starting and reference point to more detailed system models for examining DPF for accelerator purposes, we discuss work in the next section on notable modifications of an existing, essentially 0-D, reduced physics DPF system model [57]. This new DPF system model can be useful for preliminary studies of DPF acceleration potentials. The work involves making the model self-consistent from a conservation viewpoint and also by incorporating into it simple estimates of the pinch's acceleration potential based on the macroscopic fluid and instability driven inductive mechanisms discussed above. For initial beam injection calculations, we employ a test-particle method as in previous work for our DPF system model.

II. DPF Model

The self-consistent DPF model discussed here is modified notably from [57] and consists of three phases describing the rundown of the plasma sheath along the coaxial gun, the collapse or runover of the plasma radially inward towards the axis before the pinch phase, and finally the pinch phase itself. The snowplow model is employed rigorously for the first two phases, and made self-consistent with the more detailed model for the pinch phase through an energy balance between the second and third phase. Additionally, a flexible instability model is included in order to approximate acceleration voltages based on these perturbations consistently. The three phases and the equivalent circuit model are schematically illustrated by Figures 2 to 5. Here we concentrate on the equations for the DPF which is modeled as a variable inductor in the circuit with an optional serial resistor for the plasma resistance; the remainder of the circuit is easily solved given the ODEs for the DPF model. Note that the DPF model is now also self-contained as a lumped inductor and resistor from a circuit point of view and independent of the driver in contrast to [57] which required the total system energy to calculate DPF parameters. Using this system model, we can start with a simple test-particle approach to simulate particle acceleration in a DPF plasma. After describing the model, we examine sample results for the same 2.5 kJ, 12 kV DPF [58] studied in [57] which in some scenarios can provide particle accelerations in the MV range.

II.1 Rundown phase

For the rundown phase, a snowplow or piston model is employed using the average magnetic pressure. The plasma is assumed to have infinite conductivity and is infinitely thin. The dynamics in this phase are described by the following equations.

The mass accumulation of the piston as it runs down the coaxial gun is given by the flux of incoming neutral gas particles weighted by an ionization or sweep efficiency:

$$\frac{dM_Z}{dt} = \xi_Z \rho_0 V_Z \pi\left(R_o^2 - R_i^2\right) \quad (1)$$

Where M_Z is the mass of the axial plasma piston, ξ_Z is the sweep efficiency of the axial piston, ρ_0 is the static gas density, V_Z is the velocity of the axial piston, and R_i and R_o are the radius of the inner and outer electrodes. The subscript Z denotes quantities related to the axial piston. The sweep efficiency is a variable input that can be determined from experiment or more sophisticated models.

The velocity of the piston can be related to the total magnetic force pushing the piston:

$$F = \int_{R_i}^{R_o} \frac{B_\theta^2}{2\mu_0} 2\pi R dR = \frac{d(M_Z V_Z)}{dt} \text{ with } B_\theta = \frac{\mu_0 I}{2\pi R} \quad (2)$$

Where I is the total current going through the plasma and B_θ is the magnetic field pushing on the piston. Solving for the acceleration:

$$\frac{dV_Z}{dt} = \frac{1}{M_Z}\left\{\frac{\mu_0 I^2}{4\pi}\ln\left(\frac{R_o}{R_i}\right) - V_Z\frac{dM_Z}{dt}\right\} \quad (3)$$

The change in inductance of the DPF in this phase is described by:

$$\frac{dL_{DPF}}{dt} = \frac{\mu_0}{2\pi}\ln\left(\frac{R_o}{R_i}\right)V_Z \text{ since } L = \frac{\mu_0}{2\pi}\ln\left(\frac{R_o}{R_i}\right)Z \quad (4)$$

Equations (1) to (4) are sufficient to describe the dynamics of the axial piston to solve for the circuit model in the rundown phase if the plasma conductivity is assumed infinite.

For calculations that require the temperature of the piston, such as more detailed considerations of the piston resistance or modeling of the sweep efficiency, the energy of the system has to be examined. Specifically, the internal energy of the axial piston, E_Z^I, can be derived by the observation that in general the change in total energy is given by:

$$\frac{dE^T}{dt} = \left\{\frac{d(MV)}{dt}\right\}V = MV\frac{dV}{dt} + V^2\frac{dM}{dt} \quad (5)$$

Where E denotes energy, and the superscripts employed here, I, K, and T indicate internal, kinetic, and total energy. By definition, the change in kinetic energy and internal energy are:

$$\frac{dE^K}{dt} = \frac{d\left(\frac{1}{2}MV^2\right)}{dt} = MV\frac{dV}{dt} + \frac{1}{2}V^2\frac{dM}{dt} \quad (6)$$

$$\frac{dE^I}{dt} = \frac{dE^T}{dt} - \frac{dE^K}{dt} \quad (7)$$

Simplifying and solving for dE_Z^I/dt gives:

$$\frac{dE_Z^I}{dt} = \frac{1}{2}V_Z^2\frac{dM_Z}{dt} \quad (8)$$

The average temperature of the piston can be estimated, assuming temperature equilibrium, from $T_Z = (\gamma - 1)E_Z^I/N$ where γ is the ratio of specific heats and N is the total number of ions and electrons in the piston.

In general, the total energy of the plasma, $E^T(t)$, can be derived independently of the pulse generator by considering the work required to bring a variable inductor, and thus the DPF, to a specific inductance and current:

$$W(t) = \frac{1}{2}LI^2 - \frac{1}{2}LI^2(t=0) + \frac{1}{2}\int_0^t I^2\frac{dL}{dt}dt \quad (9)$$

The right-most term of the above equation is equivalent to the PdV work done on the DPF plasma:

$$\frac{dE^T}{dt} = \frac{I^2}{2}\frac{dL_{DPF}}{dt} \quad (10)$$

Energy gains due to plasma resistance can be modeled by adding the equivalent I^2R term to the RHS. Power loss due to radiation can be included similarly; typical bremmstralung losses from the dynamics in this model are small for Z=1 plasmas

II.2 Runover phase

When the axial piston reaches the end of the inner electrode or anode at Z_i, the runover phase begins. Here, the snowplow model is used again to form a radial cylindrical piston converging towards the axis and is coupled to the axial piston still moving down the chamber. The dynamics are now described by the following equations.

The change in mass and acceleration of the radial and axial pistons are given by:

$$\frac{dM_Z}{dt} = \xi_Z\rho_0V_Z\pi(R_o^2 - R^2) \quad (11)$$

$$\frac{dV_Z}{dt} = \frac{1}{M_Z}\left\{\frac{\mu_0 I^2}{4\pi}\ln\left(\frac{R_o}{R}\right) - V_Z\frac{dM_Z}{dt}\right\} \ (12)$$

$$\frac{dM_R}{dt} = -\xi_R \rho_0 V_R 2\pi R (Z - Z_i) \ (13)$$

$$\frac{dV_R}{dt} = -\frac{1}{M_R}\left\{\frac{\mu_0 I^2 (Z - Z_i)}{4\pi R} + V_R\frac{dM_R}{dt}\right\} \ (14)$$

Where R is the radius of the radial piston while its subscript denotes quantities related to the radial piston. We continue to make use of [57]'s radial piston or sheath thickness estimate, δR, to determine the end of the runover phase. Specifically, the runover phase ends and the pinch phase begins when the inner radius of the radial piston reaches the axis:

$$R - \delta R = \sqrt{R^2 - \frac{M_R}{\mu^2 \rho_0 \pi (Z - Z_i)}} = 0 \ (15)$$

Where $\mu^2 = \frac{\gamma - 1}{\gamma + 1} = 4$.

The change in inductance for this and the pinch phase is:

$$\frac{dL_{DPF}}{dt} = \frac{\mu_0}{2\pi}\left\{\ln\left(\frac{R_o}{R}\right)V_Z - \frac{(Z - Z_i)}{R}V_R\right\} \text{ since } L = \frac{\mu_0}{2\pi}\left\{\ln\left(\frac{R_o}{R_i}\right)Z_i + \ln\left(\frac{R_o}{R}\right)(Z - Z_i)\right\} \ (16)$$

Equations (11) to (16) are sufficient to describe the dynamics of the axial and radial pistons to solve for the circuit model in runover phase if the plasma conductivity is assumed infinite.

Lastly, following the derivation for the internal energy of the axial piston, the internal energy of the radial piston is provided by:

$$\frac{dE_R^I}{dt} = \frac{1}{2}V_R^2\frac{dM_R}{dt} \ (17)$$

II.3 Pinch phase

The pinch phase commences when the leading edge of the radial piston reaches the axis. As in [57], a more detailed model is used compared with the previous phases to determine the plasma behavior. The MHD continuity and radial momentum equations are solved using model velocity profiles and assuming infinite conductivity. Using these profiles and taking a spatially uniform total energy and plasma density profile, the temperature and density of the plasma as a function of time can be determined. Additionally, the thermonuclear neutron yield can be predicted although that is secondary to the current objective of particle acceleration. The difference between the work here and [57] consists of modifications which make the model consistent including an additional term in the momentum equation stemming from a derivation that uses the conservative form.

For the basic model, we employ velocity profiles as in [57]:

$$v_r(r,t) = V_R(t)\left(\frac{r}{R(t)}\right)^a \ (18)$$

$$v_z(z,t) = V_Z(t)\left(\frac{z}{Z(t) - Z_i}\right) \ (19)$$

Where R is the radius of the pinch, and V_R is the radial velocity of the pinch boundary. The lower case r and z denotes quantities inside the pinch. Z is the axial extent of the pinch and defined by the axial piston, with V_Z the velocity of the axial piston as before. This use of V_Z here is slightly different than [57] where the sound speed of the plasma was employed instead; one major consequence of this choice is that the pinch plasma mass, M_R, stays constant and the dynamics remain self-consistent. Note that the subscript R still denotes quantities in the radial or now pinch portion of the plasma. a is a profile factor for the radial velocity profile; here instead of using it a free fitting parameter, we solve for it self-consistently by remapping the kinetic energy of the radial piston at the end of the runover phase to the total kinetic energy of the pinch plasma at the start of the pinch phase using the velocity profiles above:

$$\frac{1}{2}M_R V_R^2 = \frac{M_R}{2}\left(\frac{V_z^2}{3} + \frac{V_R^2}{a+1}\right) = E_R^K \ (20)$$

Where the RHS in general can be found by $E_R^K = \int_{Z_i}^{Z}\int_0^R \frac{1}{2}\rho(v_Z^2 + v_R^2)2\pi r\, drdz$ for the pinch phase.

The continuity equation when integrated over the pinch volume is satisfied trivially using the above velocity profiles and $\rho = \rho(t)$. The density as a function of time is then merely $\rho(t) = M_R / \int_{Z_i}^{Z}\int_0^R 2\pi r\, drdz = M_R/\Gamma$, where Γ is the pinch volume.

For the momentum equation, starting out in conservative form and with current only on the plasma boundary, we have:

$$\frac{\partial(\rho\bar{v})}{\partial t} + \bar{\nabla}\cdot(\rho\bar{v}\bar{v}) = -\bar{\nabla}P \ (21)$$

We simplify for the $\hat{r}$ component taking into account the velocity profiles in Equations 18 and 19:

$$-\frac{\partial P}{\partial r} = v_r\frac{\partial\rho}{\partial t} + \rho\frac{\partial v_r}{\partial t} + 2\rho v_r\frac{\partial v_r}{\partial r} + \frac{\rho v_r^2}{r} + \rho v_r\frac{\partial v_z}{\partial z} \ (22)$$

The radial momentum equation can be solved for dV_R/dt if a pressure profile is known. Assuming a uniform total energy profile in the pinch, the pressure profile can be found by an energy balance of the DPF plasma:

$$E_{R+Z}^T(t) = E_R^K + E_R^I + E_Z^K + E_Z^I \ (22)$$

$$P(r,z,t) = \rho(\gamma-1)\left\{\frac{E_R^T(t)}{M_R} - \frac{1}{2}\left(v_z^2(z,t) + v_r^2(r,t)\right)\right\} \ (23)$$

Where $E_R^T = E_R^K + E_R^I$ is the total energy of plasma in the pinch. E_{R+Z}^T is the total energy of the plasma including the axial piston and is found via Equation 10. Since E_Z^K and E_Z^I are known from Equations (6) and (8), E_R^T can now be determined.

Taking the above and integrating over the plasma volume via Equation 22, we can solve for $\frac{dV_R}{dt}$:

$$\frac{dV_R}{dt} = -\frac{a+2}{\rho R}(P_M - P_{\mathrm{eff}}) \ (24)$$

Where $P_{\mathrm{eff}} = \rho(\gamma-1)\left\{\frac{E_R^T}{M_R} - \frac{1}{2}\left(\frac{V_Z^2}{3} + \frac{V_R^2}{2a+1}\right)\right\}$ and $P_M = \frac{\mu_0 I^2}{8\pi^2 R^2}$ is the magnetic pressure. The result is different than Equation 25 in [57] due to the inclusion of cross-terms that are apparent in a derivation starting from the conservative form of the momentum equation. These cross-terms can result in different pinch behavior.

With the pinch dynamics solved, the voltage, $V(t) = d(LI)/dt + IR$, across the pinch can be easily calculated and serves as an estimate of the accelerating potential. So far, only the inductive voltage from macroscopic fluid motion is represented; in the next section we discuss inductive voltages due to instabilities. The inclusion of finite plasma resistance would require considerations of current diffusion into the plasma and an additional $\bar{J} \times \bar{B}$ term in Equation 21.

The total D-D thermonuclear neutron yield can now also be calculated:

$$\frac{dY_n}{dt} = \int_{Z_i}^{Z}\int_{0}^{R} \frac{n_D^2}{2} < \sigma v > 2\pi r\, dr dz \ (25)$$

Where $n_D = \left(\frac{N}{2}\right)\Gamma$ is the deuterium density, and $< \sigma v >$ is the D-D averaged reaction rate determined from Equation 23. Alternatively, an average temperature, $T_{ag}(t) = (\gamma - 1)E_R^I/N$, can be used also which give typically very similar yields.

II.4 Inclusion of instability model

As discussed, instabilities have been speculated to be one of the induction based acceleration mechanisms in DPFs and Z-pinches in general. Akin to [39], we now implement a simple sub-model of a user-defined instability and consistently included it in the main model from a circuit point of view. Specifically, given a growth rate, a wave-number k/R_1, and an initial perturbation, dL_{DPF}/dt can be consistently calculated. Defining the radius of the pinch with instability as $R_{in}(z,t)$:

$$\delta R = R_1 A_1 e^{\frac{t}{\tau_g}} e^{\frac{ikz}{R_1}} \ (26)$$

$$R_{in}(z,t) = R(t) + \delta R(z,t) \ (27)$$

Where t is calculated from the start of the pinch phase, τ_g is the growth rate, A_1 is the initial seed fraction for the instability, and R_1 is set equal to R at the start of the pinch phase. R is still the pinch radius as a function of time calculated from Equation 24; we have made the assumption for simplicity that the dynamics of the mean radius is not affected other than from the change in dL_{DPF}/dt. Starting from $L_{DPF} = \int \mu_0\{\ln(R_o/R_{in})\}dz$ and Leibniz's rule, dL_{DPF}/dt is now:

$$\frac{dL_{DPF}}{dt} = \frac{\mu_0}{2\pi}\left[\ln\left(\frac{R_o}{R_{in}(Z(t),t)}\right)V_Z - \int_{Z_i}^{Z(t)} \frac{1}{R_{in}}\left(V_R + \frac{\delta R}{\tau_g}\right)dz\right] \ (28)$$

Using this definition for the change in inductance allows the effect of the instability to be consistently accounted for in the circuit model. The net voltage across the pinch based on inductive effects from both macroscopic and instability based motion can now be calculated via $d(LI)/dt$. The electric field as a function of z can also be simply determined. We note though that because we assumed negligible resistance in the pinch the voltage drop as modeled would be concentrated on the skin of the pinch.

III. Sample results from model

To demonstrate the model and compare it to the results from [57], we analyze the small DPF [58] examined in that work. Specifically, this DPF consists of a 2.5 KJ 12 KV driver, with center electrode, or anode radius of 0.9 cm, cathode radius of 5 cm, and a length of 15 cm with a net external inductance of 80 nH. The axial and radial sweep efficiencies used were 0.08 and 0.16, same as in [57] and tuned to experimental results. The calculations are useful for estimating and illustrating the plasma dynamics required to achieve high-gradient acceleration via inductive mechanisms only. We also examine from a test-particle approach beam injection and acceleration.

Figures 6 to 9 illustrate some of the results from the simple model with the instability sub-model turned off. The pinch reaches densities greater than $10^{25}/m^3$ and radial velocities greater than 50 cm/μs. The lifetime of the compression is shorter than experiment as is observed in [57] and typically in other 1-D MHD simulations. The radial velocities of the pinch are higher than typically observed in experiment also; Figure 8 gives a comparison of [57]'s pinch radial velocity profile against our model. We reached peak temperatures of 4.4 keV during the first compression, close to [57]'s 4.72 keV, but our calculated thermonuclear D-D neutron yields of 1.2 x 10^6 were significantly lower than in [57] even though the pinch dynamics are similar. Our yields are ~100 times lower than in [57] and measured in [58]; this should be expected as discussed since thermonuclear yields typically cannot account fully for measured

DPF yields. The temperature profiles are essentially flat during maximum compression. The calculated temperatures are high compared with typical experiments, although a peak temperature of 3 keV was measured for some discharges on a larger, up to 42 kJ DPF [33]. Overall there are discernable differences between our results and [57] for the same input parameters.

Concerning particle acceleration, Figure 10 gives the net accelerating voltage and the average electric field across the pinch as a function of time. Induction based fields on average of 50 MV/m are achieved from radial compression of the pinch. Figure 11 gives net acceleration of test deuterium particles started at z=0 and r=0 simulating an injected beam at various starting times, and includes the effect of ion-electron and ion-ion slowing down using the calculated density and temperatures. At these lower voltages, collisions play a role in limiting the net particle energy. The equation of motion is simply:

$$\frac{dv_z}{dt} = \frac{qE}{m_d} - (\nu_{ie} + \nu_{ii})v_z \; (29)$$

Where q is the charge of the ion, E the electric field, m_d the mass of the deuterium test particles, and ν_{ie} and ν_{ii} the ion-electron and ion-ion collision frequencies respectively.

Significantly greater accelerations can be achieved with the inclusion of strong instabilities observed in experiments [e.g. 24, 39] . We examine here what would be required to reach the MV level across this ¼ cm long plasma. For example, taking a growth rate of ½ ns, initial seed perturbation of 1%, and a k of 9, Figure 12 shows the pinch radius as a function of z and t as the plasma compresses and the instability grows. Figures 13 and 14 illustrate the substantial gains in voltage and electric fields that occur based on this instability, reaching voltages of a MV or effectively 4 MV/cm. These results suggest that the model might also describe qualitatively plasma filamentation as a source of high energy particles and be consistent with the very high gradients observed in [15].

The model and the present sample results are useful for providing estimates of accelerating potentials in the DPF due to induction based mechanisms and potentially as a tune-able guide to understanding experiments. In particular, the calculations demonstrate that acceleration gradients of ~100 MV/m are possible in a simple and low energy DPF using these mechanisms if the radial compression of the plasma and its instabilities can be tailored. However, the effective accelerating volume for the plasma examined exists on the ns timescale and can be small, providing potential challenges for beam transport and timing in regards to staged acceleration of an injected beam. Our calculations also suggest that optimizing the DPF and other fast Z-pinches for beam acceleration require different strategies compared with neutron production, such as trading pinch lifetime for sheath speed to increase induction based voltages.

IV. Conclusion

In this paper, the DPF was reviewed with an emphasis on using it as a plasma-based high-gradient accelerator with fields at the 100 MV/m level. Applications to the remote detection of high explosives and a new multi-staged acceleration concept were briefly discussed. A simple three-phase self-consistent model of the DPF geared to study acceleration potential was presented as a starting point for analysis. Initial results using the model demonstrate that induction based potentials of a MV can be achieved across a 1/4 cm long plasma in a small, 2.5 kJ, 12 KV DPF when specific instabilities occur. However, the radial velocities calculated in the model are higher than typically observed and the calculated lifetime of the pinch is shorter than measured. More detailed work is required to resolve these discrepancies and to examine in greater depth the proposed acceleration of injected beams in DPF plasmas. Nevertheless, the simple and internally consistent system model discussed here captures notable features of the DPF and its acceleration potential, and should be useful for comparisons with more sophisticated simulations.

V. References

[1] S. Fetter, V. A. Frolov, M. Miller, R. Mozley, O. F. Prilutsky, S. N. Rodionov, and R. Z. Sagdeev, "Detecting Nuclear Warheads", Science and Global Security, 1:225, 1990.
[2] T. Gozani, "Detection of Explosives and Other Threats Using Accelerator-Based Neutron Techniques", *Electrostatic accelerators: fundamentals and applications*, 445-460, Springer, 2005.
[3] M. R. Raju, "Proton Radiobiology, Radiosurgery and Radiotherapy", International Journal of Radiation Biology,67(3):237, 1995.
[4] J.W. Mather, "Investigation of the high-energy acceleration mode in the coaxial gun", Phys. Fluids Suppl., 7:5, 1964.
[5] J. W. Mather, “Formation of a High-Density Deuterium Plasma Focus”, Phys. Fluids, 8(2):366, 1965.
[6] G. Decker and R. Wienecke, “Plasma Focus Devices”, Physica, 82C:155, 1976.
[7] A. Bernard, "The dense plasma focus-a high intensity neutron source", Nucl. Instrum. Methods, 145:191, 1977.
[8] L. Soto, “New trends and future perspectives on plasma focus research”, Plasma Phys. Cont. Fusion., 47(5A):A361, 2005.
[9] D.D. Ryutov, M.S. Derzon, M.K. Matzen, “The Physics of Fast Pinches”, Rev. Mod. Phys., 72:205, 2007.
[10] C.A. Coverdale, C. Deeney, A. L. Velikovich et al, "Deuterium gas-puff z-pinch implosions on the z accelerator", Phys. Plasmas, 14:056309, 2007.
[11] H. Krompholz, L. Michel, K. Schonback, and H. Fischer, “Neutron-, Ion-, and Electron-Energy Spectra in a 1 kJ Plasma Focus”, Appl. Phys. 13(1):29, 1977.
[12] R. L. Gullickson and H. L. Sahlin, "Measurements of high-energy deuterons in the plasma focus device", J. Appl. Phys., 49(3):1099, 1978.
[13] R. Gullickson, W. L. Pickles, D. F. price, H. L. Sahlin, and T. E. Wainwright, Technical Report UCRL-81962, LLNL, 1979.
[14] M. J. Rhee, “Heavy-ion beams produced by high-voltage pulse-powered plasma focus”, Appl. Phys. Lett., 37(10):906, 1980.
[15] L. Bertalot, H. Herold, U. Jager, A. Mozer, T. Oppenlander, M. Sadowski, and H. Schmidt, "Mass and energy analysis and space-resolved measurements of ions from plasma focus devices", Phys. Lett. A, 79(5):389, 1980.
[16] M. Sadowski, H. Schmidt and H. Herold, "Time-resolved studies of deuteron beams emitted from a plasma focus", Phys. Letters 83A:435, 1981.
[17] W. Stygar, G. Gerdin, F. Venneri, and J. Mandrekas, "Particle beams generated by a 6-12.5 kJ dense plasma focus", Nuc. Fusion, 22(9): 1161, 1982.
[18] Y. Yamada, Y. Kitagawa and M. Yokoyama, "High-energy deuteron beam generated by a plasma focus device", J. Appl. Phys. 58(1): 188, 1985.
[19] W. H. Bostick, H. Kilic, V. Nardi and C. W. Powell, "Time resolved energy spectrum of the axial ion beam generated in plasma focus discharges", Nucl. Fusion 33(3):413, 1993.
[20] H. Kelly and A. Marquez, "Ion-beam and neutron production in a low-energy plasma focus", Plasma Phys. Cont. Fusion, 38(11):1931, 1996.
[21] M. Zakaullah, I. Akhtar, A. Waheed et al., “Comparative study of ion, x-ray and neutron emission in a low energy plasma focus”, Plasma Sources Sci. Technol., 7:206, 1998.
[22] S. Springham, S. Lee, and M. Rafique, “Correlated deuteron energy spectra and neutron yield for a 3 kJ plasma focus”, Plasma Phys. Cont. Fusion, 42:1023, 2000.

[23] A Patran, L C Tan, D Stoenescu, M S Rafique, R S Rawat, S V Springham, T L Tan, P Lee, M Zakaullah and S Lee, "Spectral study of the electron beam emitted from a 3 kJ plasma focus", Plasma Sources Science and Technology, 14(3):549, 2005.
[24] H. Yousefi, S. Mohanty, Y. Nakada, H. Ito, and K. Masugata, “Compression and neutron and ion beams emission mechanisms within a plasma focus device”, Phys. Plasmas, 13:114506, 2006.
[25] V.A. Gribkov, B. Bienkowska, M. Borowiecki, A. V. Dubrovsky, I. Ivanova-Stanik, L. Karpinski, R. A. Miklaszewski, M. Paduch, M. Scholz, and K.Tomaszewski, "Plasma Dynamics in PF-1000 Device under Full- Scale Energy Storage II. Fast electron and ion characteristics versus neutron emission parameters and gun optimization perspectives", J. Phys. D: Appl. Phys. 40:3592, 2007.
[26] P. Kubes J. Kravarik, D. Klir, K. Rezac, M. Scholz, M. Paduch, I. Ivanova-Stanik, L. Karpinski, K. Tomaszewski, “Determination of Deuteron Energy Distribution from Neutron Diagnostics in a Plasma Focus Device”, IEEE Trans. Plasma Science, 37(1):83, 2009.
[27] M. V. Roshan, P. Lee, S. Lee, A. Talebitaher, R. S. Rawat, and S. V. Springham, "Backward high energy ion beams from plasma focus", Phys. Plasmas 16(7):074506, 2009.
[28] C. Patou, A. Simonnet, and J. Watteau, “Measured Anisotropies of the Plasma Focus Neutron Emission Compared with Proposed Mechanisms”, Phys. Lett., 29A(1):1, 1969.
[29] M.J. Bernstein, "Deuteron acceleration and neutron production in pinch discharges", Phys. Rev. Lett., 24(13):724, 1970.
[30] M. J. Bernstein, “Evidence for Nonthermonuclear neutron production in a plasma focus discharge”, Phy. Lett., 31A(6):317, 1970.
[31] J. H. Lee, L. P. Shomo, M. Williams, and H. Hermansdorfer, “Neutron Production Mechanism in a Plasma Focus”, Phys. Fluids, 14(10):2217, 1971.
[32] J. H. Lee, L. P. Shomo, and K. H. Kim, "Anisotropy of the neutron fluence from a plasma focus", Phys. Fluids, 15(12):2433, 1972.
[33] M. J. Forrest and N.J. Peacock, "Measurement of the ion temperature in the dense plasma focus by laser beam scattering", Plasma Phys., 16:489, 1974.
[34] A. Bernard, A. Coudeville, A. Jolas, J. Launspach and J. de Mascureau, "experimental studies of the plasma focus and evidence for nonthermal processes", Phys. Fluids 18(2):180, 1975.
[35] B. Freeman, H. Kruse, R. Caird, J. King, D. Erickson, D. Bartram, C. Fowler, P. Kruse, and W. Garn, "Plasma focus experiments powered by explosive generators", Proc. 3rd International Conference on Megagauss magnetic Field Generation, Novosibirsk, USSR, 1983.
[36] F. Castillo, M. Milanese, R. Moroso and J. Pouzo, "Some experimental research on anisotropic effects in the neutron emission of dense plasma-focus devices", J. Phys. D: Appl. Phys. 30:1499, 1997.
[37] W. Leemans, and E. Esarey, "Laser-driven plasma-wave electron accelerators", Phys. Today, 62(3):44, 2009.
[38] D. Freiwald, K. Prestwich, G. Kuswa, and E. Beckner, "Neutron enhancement from relativistic electron beam-dense plasma focus interactions", Phys. Letts, 36A(4):297, 1971.
[39] O. A. Anderson, W. R. Baker, S. A. Colgate, J. Ise, and R. V. Pyle, "Neutron production in linear deuterium pinches", Phys. Rev., 110(6):1375, 1958.
[40] S. P. Gary, “Ion kinematics in a plasma focus”, Phys. Fluids, 16(7):997, 1973.
[41] S.P. Gary, "Ion acceleration in a plasma focus", Phys. Fluids, 17(11):2135, 1974.
[42] M. G. Haines, "Ion beam formation in an m=0 unstable z-pinch", Nucl. Instrum. Methods 207:179, 1983
[43] Y. Kondoh and K. Hirano, "Numerical study of an ion acceleration in a z-pinch type plasma focus", Phys. fluids 21(9), 1978.
[44] Y. Kondoh and M. Mamada, "Numerical study on charged particle accelerations in the plasma focus", Phys. Fluids, 29(2):483, 1986.

[45] U. Jager and H. Herold, "Fast ion kinetics and fusion reaction mechanism in the plasma focus", Nucl. Fusion, 27(3):407, 1987.
[46] R. Deutsch and W. Kies, "Ion acceleration and runaway in dynamical pinches", Plasma Phys. Cont. Fusion, 30(3):263, 1988.
[47] T. Haruki, H. Yousefi, K. Masugata, J. Sakai, Y. Mizuguchi, N. Makino, and H. Ito, "Simulation of high-energy particle production through sausage and kink instabilities in pinched plasma discharges", Phys. Plasmas, 13:082106, 2006.
[48] Y. Mizuguchi, J. Sakai, H. R. Yousefi, T. Haruki, and K. Masugata, "Simulation of high-energy proton production by fast magnetosonic shock waves in pinched plasma discharges", Phys. Plasmas, 14:032704, 2007.
[49] D. Potter, "Numerical studies of the plasma focus" Phys. Fluids, 14(9):1911, 1971.
[50] S. Maxon and J. Eddleman, “Two-dimensional magnetohydrodynamic calculations of the plasma focus”, Phys. Fluids 21(10):1856, 1978.
[51] K. Behler and H. Bruhns, "Three-fluid magnetohydrodynamical simulation of plasma focus discharges", Phys. Fluids, 30(12):3767, 1987.
[52] W. Stepniewski, “MHD numerical modeling of the plasma focus phenomena”, Vacuum, 76(51), 2004.
[53] S. Lee, “A new theory for the fast compressional pinch,” in Proc. 1983 College on Plasma Physics, vol. 2, Trieste, Italy, pp. 967–977.
[54] S. Lee, S. H. Saw, P. C. K. Lee, R. S. Rawat, and H. Schmidt, “Computing plasma focus pinch current from total current measurement”, Appl. Phys. Letts, 92:111501, 2008.
[55] S. Lee, “Current and neutron scaling for megajoule plasma focus machines”, Plasma Phys. Cont. Fusion, 50:105005, 2008.
[56] S. Lee, S. H. Saw, L. Soto, S. V. Springham and S. P. Moo, “Numerical experiments on plasma focus neutron yield versus pressure compared with laboratory experiments”, Plasma Phys. Cont. Fusion, 51:075006, 2009.
[57] J. H. Gonzalez, A. Clausse, H. Bruzzone, and P.C. Florido, "A lumped parameter model of plasma focus", IEEE Trans. Plasma. Sci., 32(3):1383, 2004.
[58] F. N. Beg, M. Zakaullah, M. Nisar, and G. Murtaza, "Role of anode length in a mather-type plasma focus", Modern Phys. Letts. B, 6(10):593, 1992.

Acknowledgment
We thank D. Reisman for useful technical discussions. The lead author thanks T. Houck and M. Ong for guidance. This work was performed with the auspices of the U.S. Department of Energy by Lawrence Livermore National Laboratory under contract DE-AC52-07NA27344.

Figure Captions

Figure 1: Typical DPF geometry and operation. The initial plasma sheath forms from flashover of the insulator (a), then accelerates during the rundown phase (b, c), and collapses during the runover phase (d) to form the final centimeter scale long Z-pinch at the center electrode (e). Ion beams with MeV level energies are axially emitted during the pinch (f).

Figure 2: Schematic of the rundown phase in the simple model. The snowplow model is used to describe the infinitely thin axial piston. The phase ends when the piston reaches Z_i.

Figure 3: Schematic of the runover phase in the simple model. Snowplow models are used to describe both the axial and radial pistons. The phase ends when the leading edge of the radial piston, determined via δR, reaches the axis.

Figure 4: Schematic of the pinch phase in the simple model. The snowplow model is used to describe the axial piston, while a more detailed MHD model is used to describe the pinch.

Figure 5: Equivalent circuit model of the system after commutation of the DPF with a high voltage capacitor bank using an ideal switch. The DPF coaxial gun is modeled as a variable inductor with the plasma resistance modeled as a separate resistor.

Figure 6: Current profile from simple model for the small 2.5 kJ, 12 kV DPF analyzed in [57]. The inset shows the current in detail during the pinch phase; the vertical dashed lines indicate the end of the rundown and runover phases respectively.

Figure 7: Plasma radius, length, and volume calculated from the simple model after the start of the pinch phase.

Figure 8: Plasma velocities from the simple model after the start of the pinch phase. Radial velocities from [57] with time normalized to maximum compression are included for comparison.

Figure 9: Density from simple model after the start of the pinch phase.

Figure 10: Inductive voltages and electric fields from the simple model after the start of the pinch phase. These voltages stem from radial compression and expansion of the pinch plasma without any imposed instabilities.

Figure 11: Test particle energies as a function of time for particles started at z=0, r=0 at various times using the fields from Figure 10 and the plasma parameters from the simple model. Trajectories are tracked until they leave the plasma at either $z = Z(t)$ or $z = 0$.

Figure 12: Pinch dimensions for various times after the start of the pinch phase with an instability imposed.

Figure 13: Acceleration voltages from induction with and without the instability given in Figure 12 over the 1/4 cm long plasma. A MV is reached at 1.503 ns.

Figure 14: Electric fields at t=1.503 ns as a function of plasma length for the plasma in Figure 12. The integrated voltage is 1 MV.

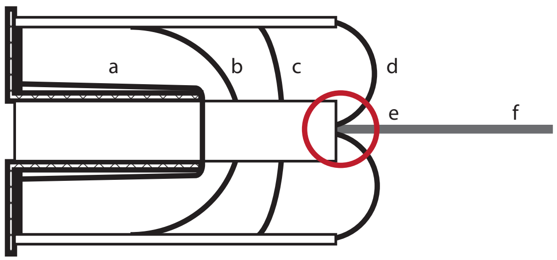
a
b
c
d
e
f

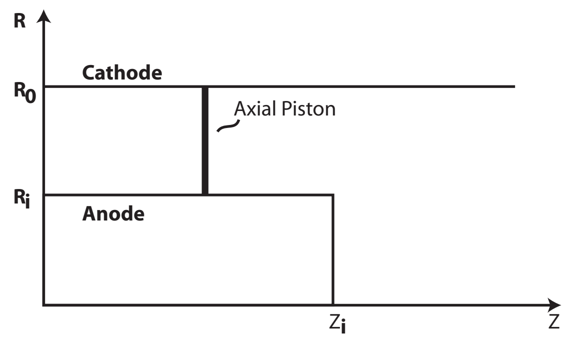
R
Cathode
R0
Axial Piston
Ri
Anode
Zi
Z

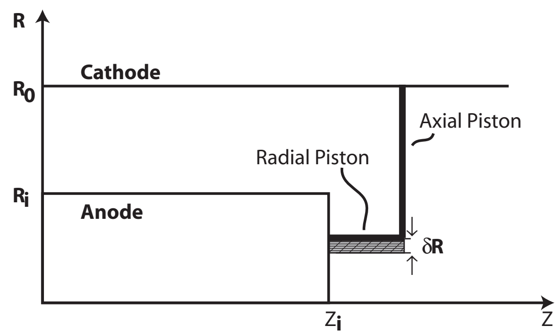
R
Cathode
R0
Axial Piston
Radial Piston
Ri
Anode
δR
Zi
Z

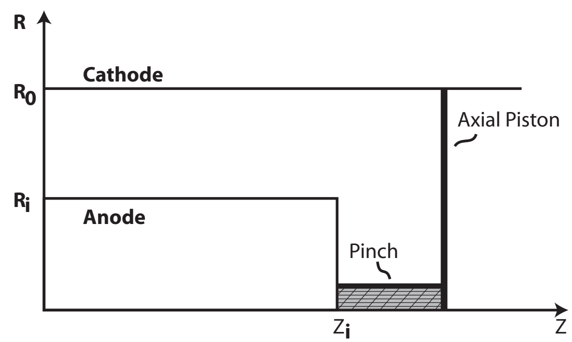
R
Cathode
R0
Axial Piston
Ri
Anode
Pinch
Zi
Z

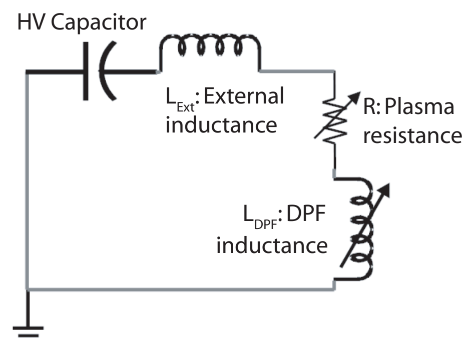
HV Capacitor
L_{Ext}: External inductance
R: Plasma resistance
L_{DPF}: DPF inductance

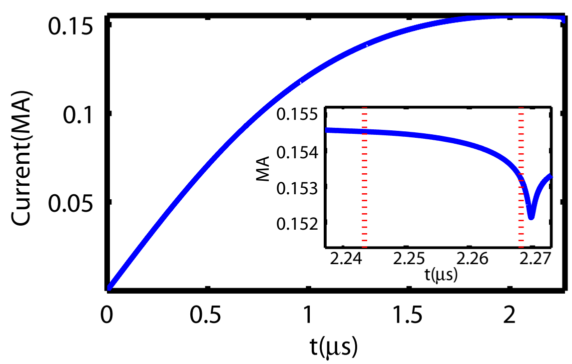
0.15
0.1
0.05
Current(MA)
0
0.5
1
1.5
2
t(μs)
0.155
0.154
0.153
0.152
MA
2.24
2.25
2.26
2.27
t(μs)

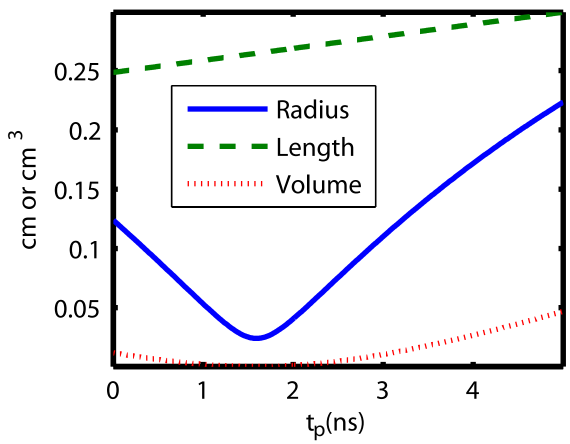

0.25
0.2
0.15
0.1
0.05
cm or cm 3
Radius
Length
Volume
0
1
2
3
4
tp(ns)

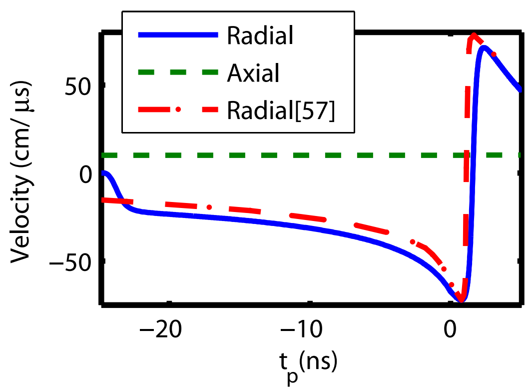

Radial
Axial
Radial[57]
Velocity (cm/ µs)
50
0
−50
−20
−10
0
t_p(ns)

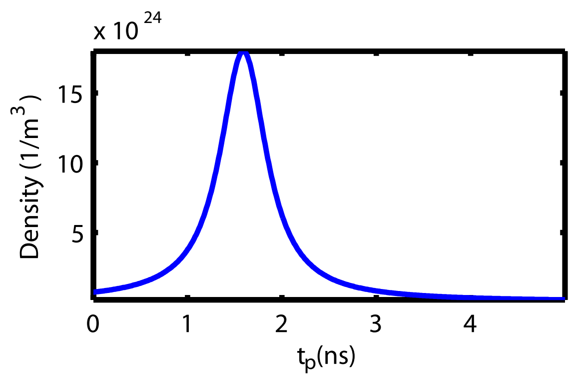
x 10 24
Density (1/m 3)
15
10
5
0
1
2
3
4
t p (ns)

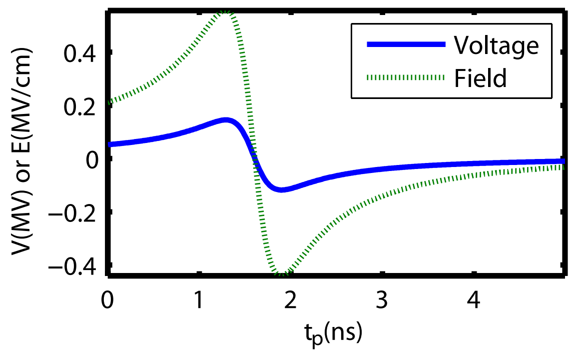
Voltage
Field
V(MV) or E(MV/cm)
0.4
0.2
0
−0.2
−0.4
0
1
2
3
4
t_p(ns)

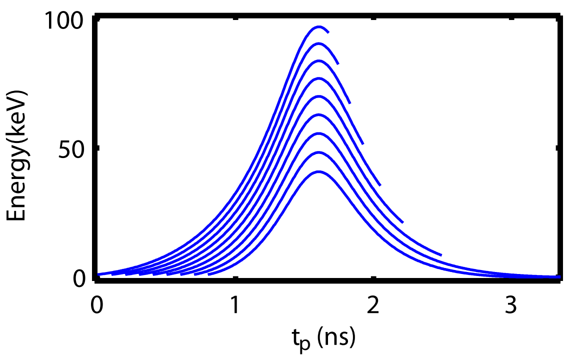
100
50
0
Energy(keV)
0
1
2
3
t_p (ns)

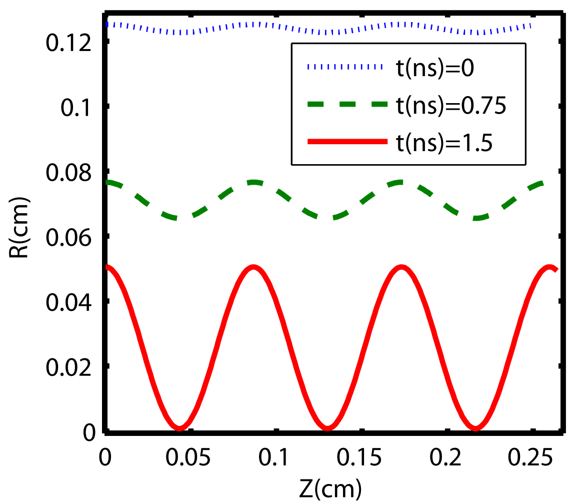

LLNL-PROC-415121

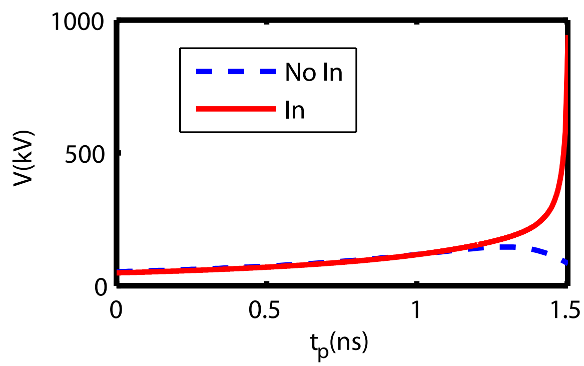
1000
500
0
V(kV)
No In
In
0
0.5
1
1.5
t_p(ns)

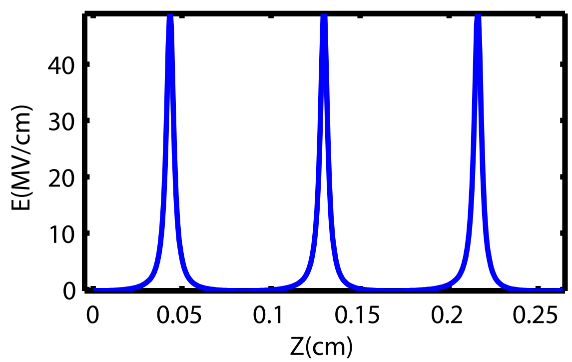
E(MV/cm)
0
10
20
30
40
0
0.05
0.1
0.15
0.2
0.25
Z(cm)